Wood Material Science & Engineering, 2015
Vol. 10, No. 2, 189–196, http://dx.doi.org/10.1080/17480272.2014.934282

Taylor & Francis
Taylor & Francis Group

ORIGINAL ARTICLE

Anatomically informed mesoscale electrical impedance spectroscopy in southern pine and the electric field distribution for pin-type electric moisture metres

SAMUEL L. ZELINKA[1], ALEX C. WIEDENHOEFT[2], SAMUEL V. GLASS[1], & FLAVIO RUFFINATTO[3]

[1]*Durability and Wood Protection Research, USDA Forest Service, Forest Products Laboratory, Madison, WI, USA,* [2]*Center for Wood Anatomy Research, USDA Forest Service, Forest Products Laboratory, Madison, WI, USA, and* [3]*Department of Agricultural, Forestry and Food Sciences (DiSAFA), University of Turin, Turin, Italy*

Abstract
Electrical impedance spectra of wood taken at macroscopic scales below the fibre saturation point have led to inferences that the mechanism of charge conduction involves a percolation phenomenon. The pathways responsible for charge conduction would necessarily be influenced by wood structure at a variety of sub-macroscopic scales – at a mesoscale – but these questions have not yet been addressed. The goal of this work is to explore if mesoscale anatomical features in wood affect impedance spectra. Small (0.5 mm diameter) needles were used as electrodes and were configured such that the line segment between the electrodes could be oriented radially, tangentially, longitudinally and in combinations of those directions in both earlywood and latewood, including comparisons of earlywood–latewood transitions. The spectra were fit to an equivalent circuit model with a constant phase element in parallel with a resistor and Warburg element that describes ionic conduction. Finite element simulations were run to examine the effect of the fringing electric field near the electrodes. The simulations revealed that the current density was concentrated at the electrodes, resulting in a lack of dependence on electrode spacing thus explaining why measurements taken with pin-type electric moisture metres are nearly independent of electrode geometry.

Keywords: *Equivalent circuit modelling, ionic diffusion, wood, impedance spectroscopy, scalar effects, wood anatomy, earlywood, latewood, mesoscale*

Introduction

Recently, Zelinka et al. proposed a new model to describe the mechanism of electrical conduction in wood based upon percolation theory (Zelinka *et al*. 2008). The model is built upon the idea that at a certain wood moisture content well below the fibre saturation point—the percolation threshold—a continuous pathway for ionic charge conduction through the wood cell walls emerges. While the concept of a continuous ion transport network in the absence of free water necessarily invokes wood microstructure, the model was based upon macroscopic impedance spectroscopy measurements in the longitudinal direction, with electrodes on the order of 1 cm^2 (Zelinka *et al*. 2007, 2008) and implicitly treated the wood material as homogeneous.

The appearance of a percolation threshold below fibre saturation point raises several interesting questions, the answers to which may give further insight into the role of moisture-facilitated ion transfer in both the corrosion of metal fasteners in wood and the degradation of wood by decay fungi. Jakes et al. recently hypothesised that the percolation threshold is physically caused by a moisture-induced glass transition of the hemicelluloses (Jakes *et al*. 2013), through which ions would be able to move. Work is currently underway to examine ion movement at the length scales of the hemicelluloses and other subcellular length scales (1 nm – 10 μm), and prior work addressed macroscopic scales.

This paper presents impedance spectroscopy measurements using 0.5 mm probes to explore if some

Correspondence: S. L. Zelinka, Durability and Wood Protection Research, USDA Forest Service, Forest Products Laboratory Madison 53726, WI, USA. Fax: 608 231 9303. E-mail: szelinka@fs.fed.us

(*Received 19 February 2014; revised 4 June 2014; accepted 10 June 2014*)

mesoscale wood anatomical features—single- to multicellular microscopic structures—affect the electrical properties above the percolation threshold but below fibre saturation in southern pine. This moisture regime was selected because it has been shown that the charge conduction mechanism in this moisture content range is ionic (Lin 1965, Zelinka *et al.* 2008) and builds upon other, recent work on impedance spectroscopy in wood and other biomaterials (Tiitta and Olkkonen 2002, Tiitta *et al.* 2003, Zelinka *et al.* 2007, 2008, Tiitta *et al.* 2010, Yang *et al.* 2013). Additionally, finite element simulations of the electric field were executed to examine how the electric field spreads across the wood mesostructure.

Experimental

Specimens were cut from clear sapwood of southern pine, specifically either longleaf or shortleaf pine (*Pinus palustris* or P. *echinata*) used in previous examinations of the electrical properties of wood (Zelinka *et al.* 2007, 2008). The specimens were cut so that they were orthogonal to the radial/tangential/longitudinal orientation of the grain in a way to maximise the distance in the tangential direction, which was limited by the curvature of the growth rings. Five blocks were cut with various axial lengths, giving electrode spacings of 10, 20, 30, 40 and 50 mm. The samples weighed 12, 20, 33, 43 and 56 g, respectively, when conditioned to the test conditions. The other dimensions of the sample were depended on the longest section we could cut without curvature in the growth rings and were approximately 25 mm (radial) by 100 mm (tangential). Three different sets of growth rings (replicates) were tested within each block.

Different longitudinal distances were examined to explore the effect of path length. For simple geometries, where the electric field is uniform, the resistance, R, scales by

$$R = \rho L / A \tag{1}$$

where L is the distance between electrodes (path length), A is the cross sectional area of the electrode and ρ is the resistivity, a material property.

Hypodermic needles (25 gauge) were used as the electrodes; the needles had an outside diameter of 0.51 mm and a wall thickness of 0.13 mm. Needle position was explored as an independent experimental variable. The needles were inserted axially to a depth of 5.5 mm, except for the shortest block (10 mm), in which the needles were inserted to a depth of 3 mm. The arrangement of the needles for a single replicate is shown in Figure 1. The needle spacing along the tangential direction was 30 mm; additional pins were added after the original measurements so that measurements along the tangential direction could be taken at spacings of 10, 20 and 30 mm. These ancillary measurements showed no trend with path length; only the 30 mm data are reported in the Results section. Table I details the needle positions used to measure the combination of the three primary directions of the wood.

Specimens were conditioned in an environmental chamber with set points of 27 ± 1°C and 95 ± 3% RH until successive mass readings were within the uncertainty of the balance (0.2 mg). The resulting moisture content was 20.6%. Impedance spectra were taken in the laboratory at 22°C and 50% RH+/–5%. Preliminary impedance spectra had problematically low repeatability, which was traced to the specimens drying during the period over which the measurements were taken; the mass changed as much as 1% over the 8 hours required to take a set of measurements. To improve the repeatability, specimens were coated with neoprene paint (Republic Powdered Metals Inc., Beachwood, OH), which greatly reduced the rate at which specimens lost moisture and thus improved the repeatability of the measurements; the neoprene paint was non-conductive and did not affect the impedance spectra. After coating, the samples lost less than 0.1 g during the measurement, which results in a change in moisture content of less than 1% during the test, in the worst-case scenario. Therefore, the moisture content of sample during testing was constant and equal to the moisture content of the wood equilibrated at 27°C and 95% RH.

Impedance spectra were collected with a Gamry PCIGamry® PCI4-300 potentiostat (Gamry Instruments, Warminster, Pennsylvania). Root mean

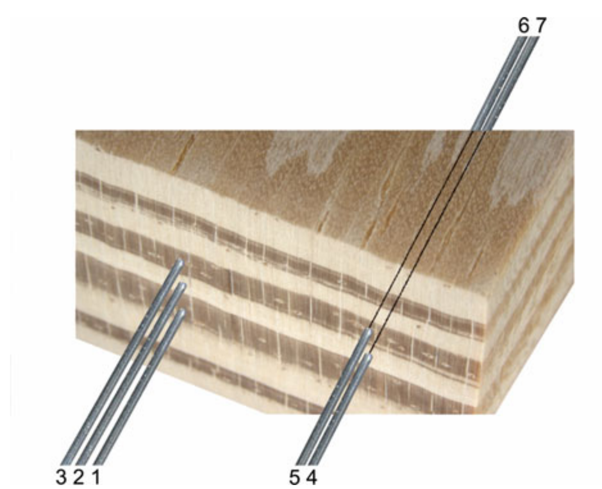

Figure 1. Schematic illustration of the configuration of the electrodes (not to scale). The distance between the electrodes was an experimental variable. The needles were arranged such that every combination of radial/tangential/longitudinal measurement could be taken (see Table I)

Table I. Summary of measurements taken for each 'replicate', needle numbers correspond with the locations in Figure 1.

Direction	Tissue	Needle 1–Needle 2 (see Figure 1)	Explanation
T	*e*	2–4	Tangential, earlywood
T	*l*	3–5	Tangential, latewood
R	*e*1–l1	2–3	Radial, earlywood of Year 1 to latewood of same Year
R/T	*e*1–l1	2–5	Tangential and radial, from the earlywood of Year 1 to latewood of same year
L	*e*	4–7	Longitudinal, earlywood
L	*l*	5–6	Longitudinal, latewood
R	l1–*e*2	1–2	Radial, latewood of Year 1 to the earlywood of the next year
R	l1–l2	1–3	Radial, latewood of Year 1 to latewood of the next year
L/T	*e*	2–7	Longitudinal and tangential, earlywood
L/T	*l*	3–6	Longitudinal and tangential, latewood
L/R	*e*1–l1	4–6	Longitudinal and radial, from the earlywood of Year 1 to latewood of same year
L/T/R	*e*1-l1	2–6	Longitudinal, tangential and radial, from the earlywood of Year 1 to latewood of same year

T/R/L refer to the tangential, radial and longitudinal directions respectively. '*e*' and 'l' refer to the earlywood and latewood, respectively, and the subscript indicates which year the growth ring is from. For example, R_{l1-e2} refers to a measurement in the radial direction from the latewood of one year to the earlywood of the next year.

square amplitude of applied voltage was 10 mV, and the range of frequencies tested was 3×10^5 Hz to 1×10^{-1}Hz with 10 frequencies measured per decade change in frequency. Because no reference electrode was used, the lead for the reference electrode was attached to the counter electrode, which resulted in all measurements being taken at zero volts with respect to open circuit potential.

Spectra were fit with the equivalent circuit model shown in Figure 2. The model contains a resistor ($R2$) in parallel with a constant phase element (CPE-symbol Q) which describes the relaxation of charge carriers (presumably ions) within the wood; a CPE is a capacitor with a distribution of relaxation times and is frequently observed in non-homogeneous systems (Cole and Cole 1941). The model also contains a Warburg (W) element that describes the long-range diffusion of ions; the Warburg element dominates at low frequencies and is responsible for the linear region in Figure 3. Finally the model contains ($R1$), which can describe any extra interfacial resistance; however, in all measurements, the model was best fit with $R1 = 0$.

Results

Figure 3 shows a typical mesoscale impedance spectrum taken along the longitudinal direction, within the earlywood of a single growth ring, with a 20 mm electrode spacing. All spectra exhibited a single time constant at higher frequencies and a low frequency linear region. These characteristics are consistent with macroscopic impedance spectra taken above the percolation threshold (and included in Figure 2 for reference) (Zelinka *et al.* 2008).

A CPE (Q) was used to model the ionic relaxation. Whereas a perfect capacitor has a ω^{-1} behaviour, a CPE has a ω^{-n} response, where n is an additional fitting parameter that physically describes the width of distribution of relaxation times. We found that in approximately 80% of the spectra, the best fit was obtained with $n = 1$, and that the average value of n over all spectra was 0.99.

Six of the measurements in Table I do not depend on the longitudinal distance. For these, measurements on all five of the blocks can be compared and have a total of 15 replicates (3 per block × 5 blocks). We present these data in Figure 4 as a box-and-whiskers plot where the edges of the box are the 25th and 75th percentiles and the centreline is the median. The notches on the box represent confidence intervals of the medians; the medians are significantly different at the 5% level when they do not overlap. For the CPE coefficient, time constant and Warburg coefficient, the intervals are larger than the box, (see, for example, R_{l1-e2} of in the Warburg coefficient plot).

The remaining six measurements depended on the longitudinal distance and are plotted as a function of such in Figure 5. The filled symbols represent measurements taken in the earlywood, open symbols in the latewood and measurements in the radial direction are plotted with crosses. These

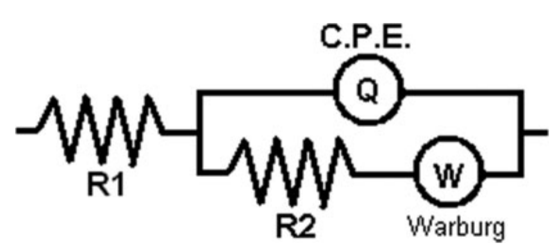

Figure 2. Equivalent circuit model used to interpret the impedance spectra; $R1$, the interfacial resistance, was allowed to vary but was found to be zero in all cases

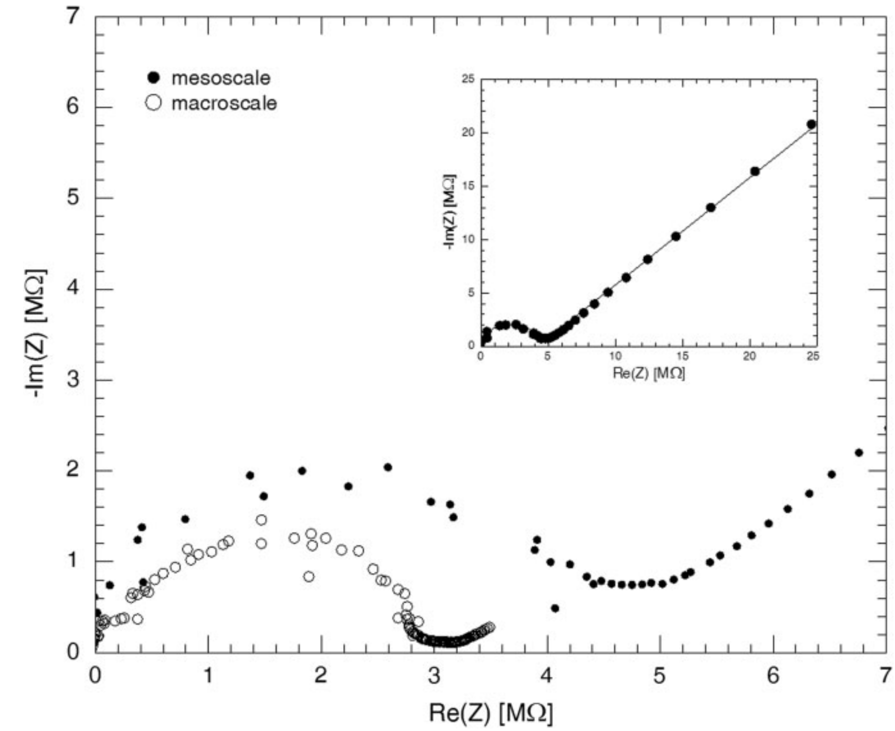

Figure 3. Example impedance spectrum (closed symbols, longitudinal, earlywood, 20 mm electrode spacing) compared with the macroscale data (open symbols, 25 mm electrode spacing). The inset shows the entirety of the mesoscale data with equivalent circuit model fit overlaid

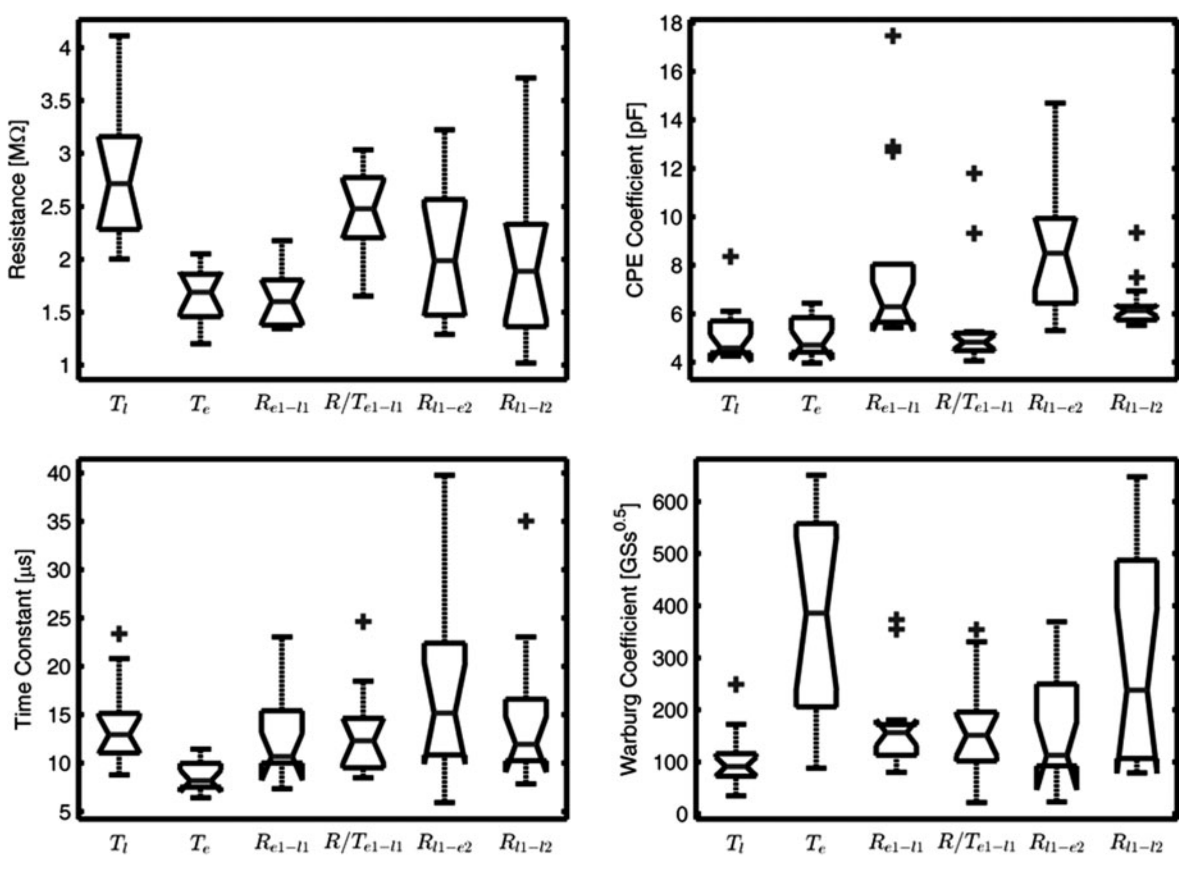

Figure 4. Model fit parameters for the measurements taken in the tangential and/or radial directions. Clockwise from upper left: Resistance, CPE coefficient, Warburg coefficient and time constant. The whisker length represents the maximum or minimum value that is not an outlier, which was determined as a value greater than q3 + w(q3 − q1) or smaller than q1 − w(q3 − q1), where q1 and q3 are the 25th and 75th percentiles, respectively. Outliers are represented by '+' symbols

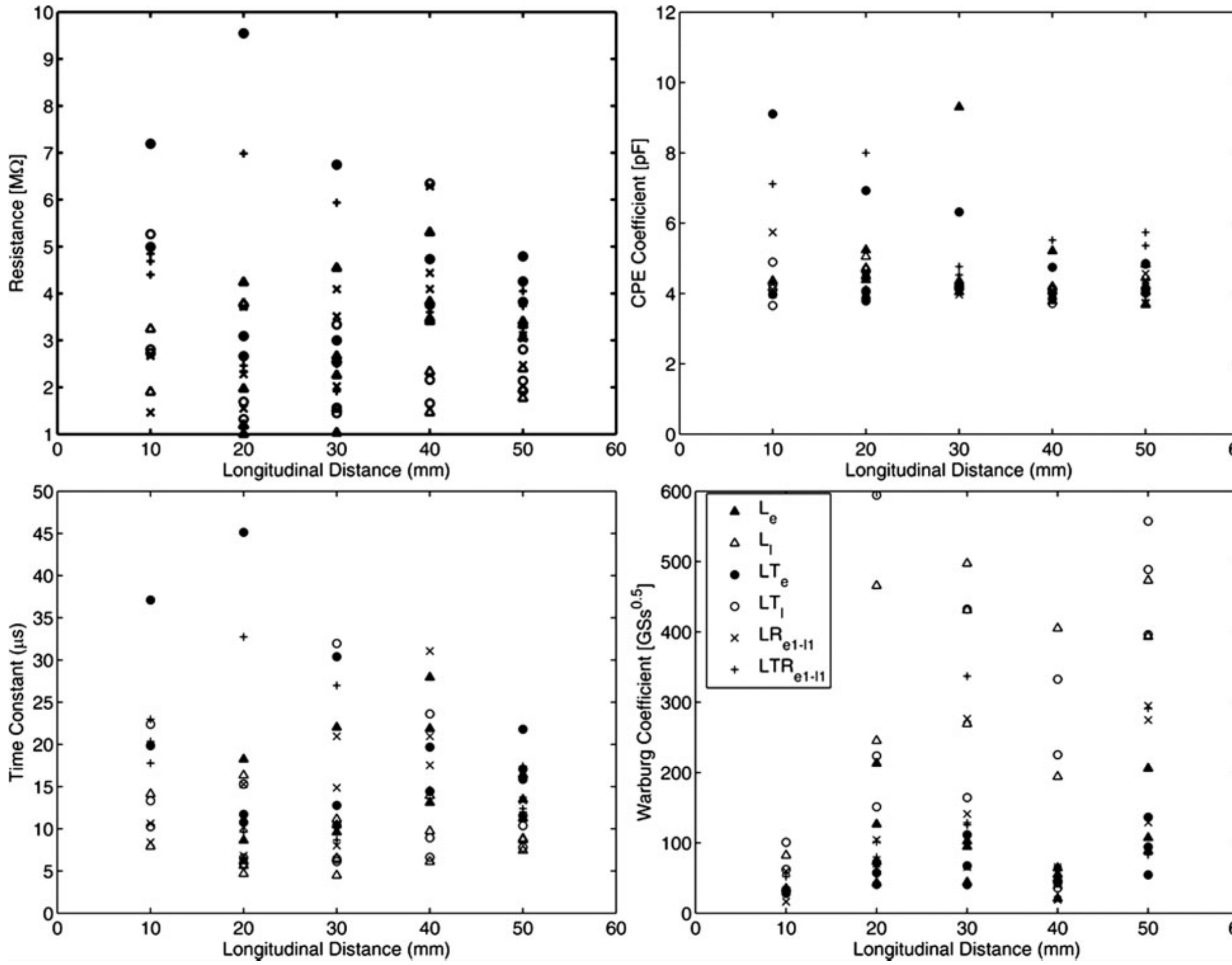

Figure 5. Model fit parameters as a function of electrode spacing in the longitudinal distance. Clockwise from upper left, Resistance, CPE coefficient, Warburg coefficient and time constant

measurements do not show any apparent trend with longitudinal distance. Least-squares fitting (not shown) confirms the lack of dependence; for resistance, the highest R^2 value was 0.17 ($L/R_{e1\text{-}l1}$) and most of them were less than 0.1 with the lowest R^2 value of 0.004 (L_l). The additional measurements at 10 mm and 20 mm along the tangential direction also did not exhibit a dependence on path length.

To better understand the effect of our electrode geometry on the results, we used finite element modelling (FEM) to solve the Poisson equation:

$$-\sigma \nabla^2 V = 0 \qquad (2)$$

where σ is the conductivity ($1/\rho$) and V is the electric potential. Simulations were run using the partial differential equation toolbox in Matlab™ (MathWorks, Natick, MA) and assumed a homogeneous media. The results yielded the electric field $\vec{E}$ over the entire domain. The current was calculated by integrating the gradient of the electric field over the symmetry plane between the electrodes.

The results (current density) of an example simulation (physical dimensions of 500 mm wide by 100 mm tall with an electrode spacing of 50 mm) are overlaid with a micrograph of the wood structure near an electrode in Figure 6. Each of the contours of the graph represent a 10% decrease in current density. From the figure, it can be seen that 80% of the current density is concentrated in the first 2 mm near the electrode and more than 10% of the current density is concentrated in the cells that have been crushed by the insertion of the needle.

Discussion

In general, the results did not depend upon path length as predicted by Equation 1. However, the electric field was clearly non-uniform (Figure 6). Therefore, we ran additional simulations to compare our results against predicted behaviour given our geometry.

The simulations used a domain with physical dimensions of 500 mm wide by 100 mm tall and

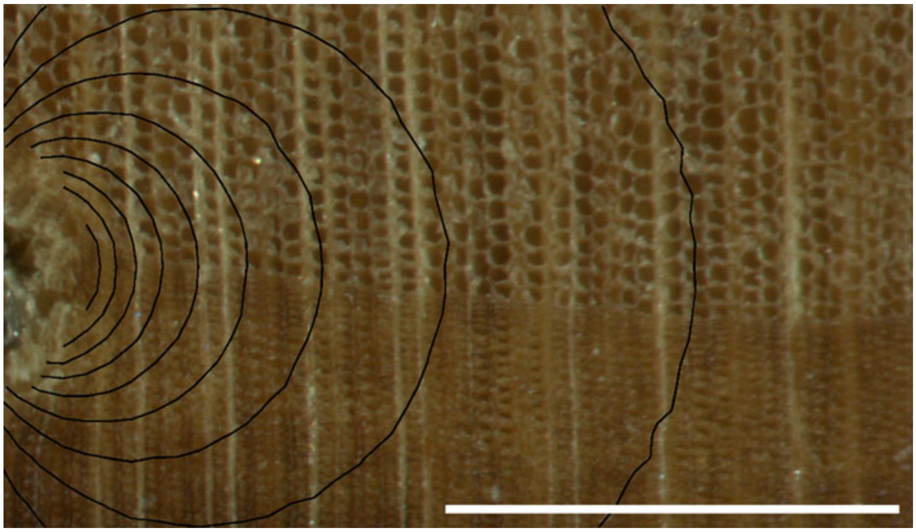

Figure 6. Current density (from a FEM simulation) overlaid on a micrograph of the wood structure (the scale bar represents 1mm). Each of the contours represents a 10% drop in current density

assumed homogenous properties across the domain. The assumption of a homogenous domain is clearly an oversimplification since the cell lumina are non-conductive, and there are likely differences between the middle lamella and secondary cell walls. The simplification to a homogenous domain was used since the goal of the simulations was to examine relative differences in the apparent resistivity with different electrode spacings on the order of 0.01 m and above, and these homogeneities occur at length scales of 0.000 01 m and below. The electrodes were modelled as circles with a diameter of 0.5 mm. Eight simulations were run at 8 electrode spacings: 10, 20, 30, 40, 50, 125, 250 and 500 mm on centre. Since we were interested in the relative changes in resistance caused by electrode spacing, the conductivity was set to one by normalising all of the measurements to the resistance measured at the 10 mm spacing, the simulations become independent of the material properties like conducitivity.

Figure 7 shows the electric potential and current density from an example simulation and each sub-figure is subdivided into 20 contours. It is clear from the simulation that 80% of the current is concentrated in the first 2 mm near the two electrodes. Given that 80% of the current is concentrated within the first 2 mm even in the 10 mm electrode spacing, it is not surprising that the resistance did not strongly depend upon electrode spacing from 10–50 mm. Figure 8 shows the relative resistance calculated from the FEM simulations as a function of electrode spacing. According to the simulations, the resistance at the 50 mm electrode spacing should be about 1.6 times larger than the resistance at the 10 mm electrode

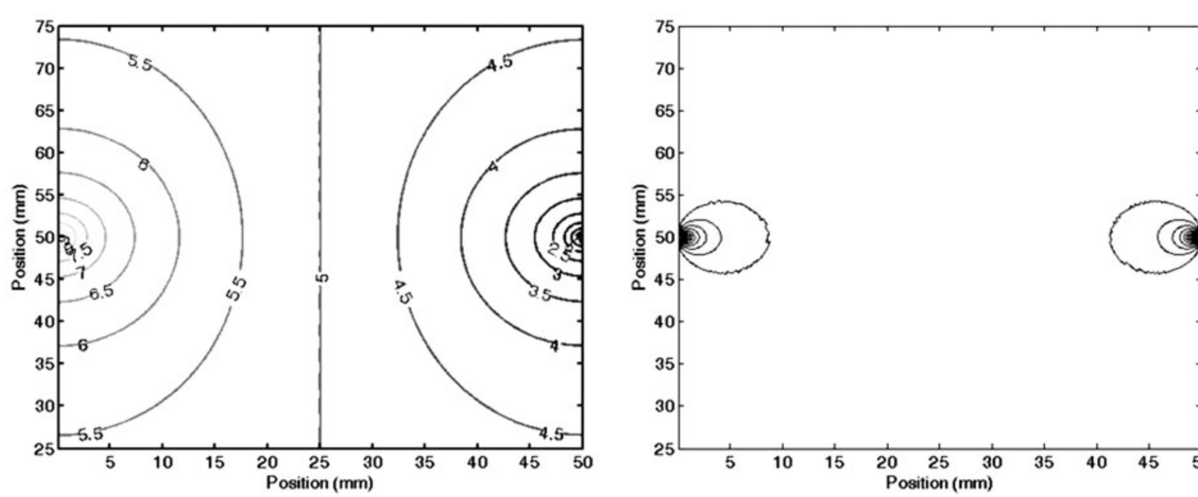

Figure 7. Example results from the FEM simulation presented as contour maps of the electric potential (left) and current density in arbitrary units where each contour represents 1/20th of the magnitude (right)

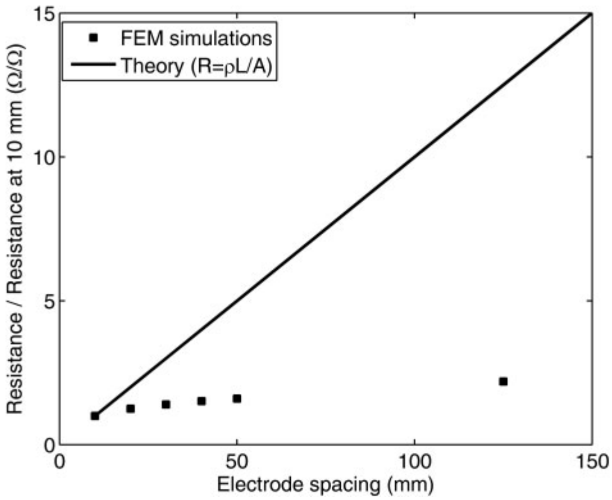

Figure 8. FEM simulations of the resistance for different electrode spacings divided by the simulated resistance at 10 mm. The traditional $R = \rho L/A$ for uniform electric field is included for reference

spacing, as opposed to the five times larger predicted by Equation (1) for a uniform electric field. The simulations predict a small increase in resistance with increasing electrode spacing. However, the error bars in our measurements are much larger than the small increase the simulations suggest, which would explain why we see no apparent trend in any model parameters with increasing longitudinal distance (Figure 5).

The fact that the electric field is concentrated around the electrodes has important implications for these measurements and also electric moisture metres for wood, widely used in wood industry and for wood technological applications. Our initial goal was to examine the effect of mesoscale wood anatomical properties on the electrical properties of wood. The high current density in the immediate vicinity of the electrodes, and the extremely low current density at any appreciable distance from the electrodes, results in a local sampling of the electrical properties adjacent to the electrodes rather than a uniform sampling of a path between the electrodes. These simulations are consistent with our experimental observations in which measurements were independent of path length when electrodes were separated by more than 10 mm. This is in turn consistent with the general consensus in the wood technological literature (James 1963, 1988, Forsén and Tarvainen 2000) that suggests similar results of pin-distance independence, without ever addressing the basic physics and wood science underlying the phenomenon.

For needle configurations in which both were in the same tissue (e.g. in the earlywood of the same growth ring), our results are essentially characterisations of small amounts of that tissue. For instance, the resistance of the earlywood was higher than that of the latewood, and this was most evident when measuring in the tangential direction. The latewood had a lower resistance, a faster time constant and a higher Warburg coefficient than the earlywood; all of which are consistent with more facile ion movement in the latewood. The ratio of the resistance of the earlywood to that of the latewood is approximately scaled with the inverse of the ratio of the specific gravity of the earlywood to that of the latewood. Resistance measurements in which one electrode was in the earlywood and the other in the latewood at a distance of 30 mm (*R*/*T* configuration) are intermediate to the tangential earlywood or latewood resistances. In this configuration, one electrode was in the higher-resistivity earlywood and the other electrode was in the lower-resistivity latewood, and the electrodes were widely separated (compared to the *R* configuration, where the separation was approximately 2 mm), thus the resulting measurement was the average of the two tissues.

Another interesting aspect of mesoscale measurements is that the CPE exponent, which represents the distribution of time constants, was found to be 1 in almost all cases, and therefore, the CPE can be replaced by a true capacitor when modelling electrical behaviour at the mesoscale. In contrast, in previous macroscale measurements (Zelinka 2006; electrode diameter 13 mm), Zelinka et al. found that the CPE exponent ranged from 0.71 to 0.97 with an average of 0.84. This suggests that any given earlywood or latewood band has a single time constant; the distribution of time constants observed in the macroscale measurements was caused by averaging across several growth rings with different time constants.

From a practical standpoint, the results of the FEM simulations can also be applied to pin-type electric moisture metres (pin diameter 2.5 mm). In developing the electric moisture metre, James (James 1963, 1988) observed that the measured resistance was not sensitive to the distance between the pins. This is consistent with our simulations (Figure 7) and measurements (Figure 5). James stated that ‘the observed resistance is almost exclusively in the thin shell of wood that is immediate contact with the pin’, although it was unclear whether this was to be interpreted to mean that there was a large contact resistance between the pins and the wood, or rather that the current decays rapidly near the electrode. Our simulations and the observation that the model parameter R1 was equal to zero show that it is the latter. Furthermore, the simulations give insight into the size and shape of the "shell" that James (James 1963, 1988) had proposed (Figure 6).

Conclusions

Mesoscale electrical impedance spectra were taken in the radial, tangential and longitudinal directions of southern pine. Electrode configurations tested electrical properties within single growth rings and across adjacent growth rings. The spectra were fit to an equivalent circuit model with a CPE in parallel with a resistor and a Warburg element. A resistor ($R1$) was added in the series to account for contact resistance between the electrode and the wood surface. Although this parameter was allowed to vary, the best fit occurred when this resistor had a value of zero. This suggests that there was negligible contact resistance in these measurements. The CPE represents a capacitor with a distribution of time constants. Unlike macroscale measurements which had a broad distribution of time constants, we found that in nearly all cases the data were best fit when the CPE exponent was unity (i.e. perfect capacitor behaviour).

Impedance spectra did not vary with path length along or across the grain, but the resistance of the earlywood was higher than that of the latewood in all the configurations measured. The ratio of earlywood to latewood resistance scaled approximately with the inverse ratio of the earlywood to latewood specific gravity. The apparent insensitivity of our test apparatus to factors other than earlywood or latewood was related to the size and geometry of our electrodes. A finite element model, with assumptions of a solid, isotropic material, indicated that the high radius of curvature of the electrodes gave rise to an electric field concentrated in their immediate vicinity. The concentration of an electric field adjacent to a cylindrical electrode is sufficient to explain the spacing-independence of pins in electric moisture metres used in the wood products industry.

Funding

S.Z. acknowledges funding from the Presidential Early Career Awards for Scientists and Engineers (PECASE). Research was funded by the Forest Products Laboratory of the US Forest Service. The research was performed by government researchers on official time and therefore is part of the public domain and not subject to copyright.

References

Cole, K. S. and Cole, R. H. (1941) Dispersion and absorption in dielectrics I. Alternating current characteristics. *Journal of Chemical Physics*, 9, 341–351.

Forsén, H. and Tarvainen, V. (2000) *Accuracy and Functionality of Hand Held Wood Moisture Content Meters* (Espoo, Finland: Technical Research Centre of Finland Espoo).

Jakes, J. E., Plaza, N., Stone, D. S., Hunt, C. G., Glass, S. V. and Zelinka, S. L. (2013) Mechanism of transport through wood cell wall polymers. *Journal of Forest Products and Industries*, 2, 10–13.

James, W. L. (1963) *Electric Moisture Meters for Wood. U.S. Forest Service Research Note FPL-08* (Madison, WI: US Forest Service Forest Products Laboratory).

James, W. L. (1988) *Electric Moisture Meters for Wood. Forest Products Laboratory General Technical Report FPL-GTR-6* (Madison, WI: US Forest Service Forest Products Laboratory).

Lin, R. T. (1965) *A Study of Electrical Conduction in Wood* (Syracuse, NY: State College of Forestry at Syracuse University).

Tiitta, M., Kainulainen, P., Harju, A. M., Venäläinen, M., Manninen, A. M., Vuorinen, M. and Viitanen, H. (2003) Comparing the effect of chemical and physical properties on complex electrical impedance of scots pine wood. *Holzforschung*, 57, 433–439.

Tiitta, M. and Olkkonen, H. (2002) Electrical impedance spectroscopy device for measurement of moisture gradients in wood. *Review of Scientific Instruments*, 73, 3093–3100.

Tiitta, M., Tomppo, L. and Lappalainen, R. (2010) Combined acoustic and electric method for monitoring wood drying process: A review. *Wood Material Science and Engineering*, 5, 78–83.

Yang, L., Wang, X., Funk, T., Gates, R. and Zhang, Y. (2013) Impedance-based moisture sensor design and test for gas-phase biofilter applications. *Transactions of the ASABE*, 56, 1613–1621.

Zelinka, S., Glass, S. and Stone, D. (2008) A percolation model for electrical conduction in wood with implications for wood-water relations. *Wood and Fiber Science*, 40, 544–552.

Zelinka, S. L. (2006) Equivalent circuit modeling of Southern pine. Masters Thesis. University of Wisconsin Madison.

Zelinka, S. L., Rammer, D. R. and Stone, D. S. (2008) Impedance spectroscopy and circuit modeling of Southern pine above 20% moisture content. *Holzforschung*, 62, 737–744.

Zelinka, S. L., Stone, D. S. and Rammer, D. R. (2007) Equivalent circuit modeling of wood at 12% moisture content. *Wood and Fiber Science*, 39, 556–565.